Designing and Testing of Concrete Bridge Decks Reinforced with Glass FRP Bars

Brahim Benmokrane[1]; Ehab El-Salakawy[2]; Amr El-Ragaby[3]; and Thomas Lackey[4]

Abstract: In addition to their high strength and light weight, fiber-reinforced polymer (FRP) composite reinforcing bars offer corrosion resistance, making them a promising alternative to traditional steel reinforcing bars in concrete bridge decks. FRP reinforcement has been used in several bridge decks recently constructed in North America. The Morristown Bridge, which is located in Vermont, United States, is a single span steel girder bridge with integral abutments spanning 43.90 m. The deck is a 230 mm thick concrete continuous slab over girders spaced at 2.36 m. The entire concrete deck slab was reinforced with glass FRP (GFRP) bars in two identical layers at the top and the bottom. The bridge is well instrumented at critical locations for internal temperature and strain data collection with fiber-optic sensors. The bridge was tested for service performance using standard truck loads. The construction procedure and field test results under actual service conditions revealed that GFRP rebar provides very good and promising performance.

DOI: 10.1061/(ASCE)1084-0702(2006)11:2(217)

CE Database subject headings: Bridge decks; Bridges, concrete; Fiber reinforced materials; Fiberglass; Field tests; Fiber optics.

Introduction

The expansive corrosion of steel reinforcing bars stands out as a significant factor limiting the life expectancy of reinforced concrete structures. In North America, significant temperature fluctuations and the use of deicing salts exacerbate the phenomenon in parking garages and on bridge decks. Indeed, North America's freeze–thaw cycles and heavy salt applications subject roads and bridges to quite severe environmental conditions. Furthermore, the expansive corrosion of steel causes cracking and spalling of concrete bridge decks, resulting in major rehabilitation costs and traffic disruption (Yunovich and Thompson 2003). Problems related to expansive corrosion could be resolved by protecting the steel reinforcing bars from corrosion-causing agents or by producing rebars made of noncorrosive materials. Fiber-reinforced polymer (FRP) composite reinforcement is one such alternative, which has been used successfully in many industrial applications and more recently has been used as concrete reinforcement in bridge decks and other structural elements (Rizkalla and Tadros 1994; Saadatmanesh and Ehsani 1996; Japan Concrete Institute 1997; Benmokrane and Rahman 1998; Rizkalla et al. 1998; Hassan et al. 1999; Humar and Razaqpur 2000; Khanna et al. 2000; Tadros 2000; Benmokrane et al. 2001a; Steffen et al. 2001; Yost and Schmeckpeper 2001; Benmokrane and El-Salakawy 2002; Bradberry and Wallace 2003). Using noncorrosive FRP reinforcing bars in concrete bridge decks can extend service life, reduce maintenance costs, and improve life-cycle cost efficiency. Moreover, FRP rebars may also reduce construction costs by eliminating the need for membrane and pavement items. Typical concrete bridge deck slabs in Canada and the United States consist of two mats of steel bars (e.g., traditional black steel, galvanized steel, and epoxy-coated steel bars) with an increased concrete cover (up to 75 mm at the top), a membrane, and pavement as added corrosion protection. It should be noted that the concrete structural deck slab is the bridge component most vulnerable to corrosion deterioration because it is directly exposed to high concentrations of chlorides used for snow and ice removal.

Since glass fiber-reinforced polymer (GFRP) rebar is more economical than the available types (carbon and aramid) of FRP rebars, it is more attractive for infrastructure applications and to the construction industry. In fact, several concrete bridge decks have recently been built in North America with GFRP composite rebars (GangaRao et al. 1997; Bradberry 2001; Stone et al. 2001; Nanni and Faza 2002; El-Salakawy and Benmokrane 2003; El-Salakawy et al. 2003b; Huckelbridge and Eitel 2003). The new Canadian Highway Bridge Design Code *CAN/CSA-S6-00* (CSA Int. 2000) includes Section 16 on using FRP composite bars as nonprestressed and prestressed reinforcement for concrete bridges (slabs, girders, and barrier walls). Furthermore, several codes and design guidelines for concrete structures reinforced with FRP bars have been published recently (ISIS 2001; CSA Int. 2002; ACI 2003).

Through the NSERC Industrial Research Chair in Fiber-Reinforced Polymer Composite Reinforcement for Concrete Infrastructures, a joint effort with the Ministry of Transportation of Quebec (MTQ) was established to develop and implement FRP reinforcement for concrete bridges. This effort initially

[1]NSERC Research Chair Professor in FRP Reinforcement for Concrete Structures, Dept. of Civil Engineering, Univ. of Sherbrooke, Sherbrooke PQ, Canada J1K 2R1 (corresponding author). E-mail: brahim.benmokrane@usherbrooke.ca

[2]Research Associate Professor, Dept. of Civil Engineering, Univ. of Sherbrooke, Sherbrooke PQ, Canada. E-mail: ehab.elsalakawy@usherbrooke.ca

[3]PhD Candidate, Dept. of Civil Engineering, Univ. of Sherbrooke, Sherbrooke PQ, Canada J1K 2R1.

[4]Bridge Engineer, Vermont Agency of Transportation, Montpelier, VT.

Note. Discussion open until August 1, 2006. Separate discussions must be submitted for individual papers. To extend the closing date by one month, a written request must be filed with the ASCE Managing Editor. The manuscript for this paper was submitted for review and possible publication on January 9, 2004; approved on December 7, 2004. This paper is part of the ***Journal of Bridge Engineering***, Vol. 11, No. 2, March 1, 2006. ©ASCE, ISSN 1084-0702/2006/2-217–229/$25.00.

Table 1. Properties of No. 19 GFRP Reinforcing Bars

Bar diameter (mm)	Bar area (mm^2)	Modulus of elasticity (GPa)	Tensile strength (MPa)	Ultimate strains (%)
18.72	275	40±1	597±24	1.49±0.1

Note: ±XX=standard deviation.

focused on developing and improving glass/carbon composite bars (Benmokrane et al. 2002a,b). After achieving satisfactory laboratory results on concrete deck slab and bridge barrier wall prototypes reinforced with these bars (El-Salakawy et al. 2003a; El-Salakawy and Benmokrane 2004), the focus shifted to field applications to push the technology forward (El-Salakawy and Benmokrane 2003; El-Salakawy et al. 2003b). These field applications help validate and improve existing design codes and guidelines, establish construction details, and evaluate the performance of FRP rebars under actual service loading and environmental conditions.

This paper presents an innovative field application of GFRP bars as reinforcement in the concrete deck slab of the Morristown Bridge recently built in Vermont, United States. This bridge was selected as a demonstration project based on the Innovative Bridge Research and Construction (IBRC) (USDOT 2002) program established by the Federal Highway Administration (FHwA). The bridge was instrumented at critical locations to monitor the bridge behavior from construction startup to several years after opening to traffic. The results presented in this paper focus on the field tests that were carried out on the bridge approximately 1 year after it was opened to traffic. An example for calculating GFRP reinforcement for the deck slab (top and bottom mats) according to the available codes is also provided in the Appendix.

Tensile Properties of GFRP Bars Used in Bridge Deck Slab

Table 1 provides the tensile properties of the No. 19 (18.7 mm diameter) sand-coated glass FRP bars used to reinforce the deck slab of the Morristown Bridge. These GFRP bars (see Fig. 1) are manufactured by combining the pultrusion process with an in-line coating process for the outside sand surface. The GFRP bar is made from high-strength E-glass fibers (75% fiber by volume) with a vinyl ester resin, additives, and fillers. The glass fibers give the bar mechanical strength, while the resin matrix (resin, additives, and fillers) provides corrosion resistance in harsh environments. Durability data on this type of GFRP bar, obtained from extensive laboratory accelerated aging tests, including immersion in alkaline solution, sustained tensile stress, elevated temperature, and freeze–thaw cycles, can be found elsewhere (Benmokrane et al. 2001b, 2002a; Wang et al. 2002; Laoubi et al. 2003; Nkurunziza et al. 2003).

Deck Slab Design

Normal-weight high-performance concrete with an average 28 day compressive strength of 27 MPa was used. Design forces were determined by one-way analysis of the slab and using empirical equations (AASHTO 1994, 2000). Slab analysis assumed a 1.0 m wide strip of the transverse slab continuous over knife-edge supports representing the main girders. HS-25 truck loading was used as the design load. Crack width, rather than strength and allowable stress limits, was the controlling design factor and determined bar size and spacing for the GFRP bars in the deck. In this case, the choice of maximum acceptable crack width was 0.5 mm (Bradberry 2001). Design calculations for the Morristown Bridge deck slab are given in the Appendix. The following section presents some details about the construction and reinforcement of this bridge.

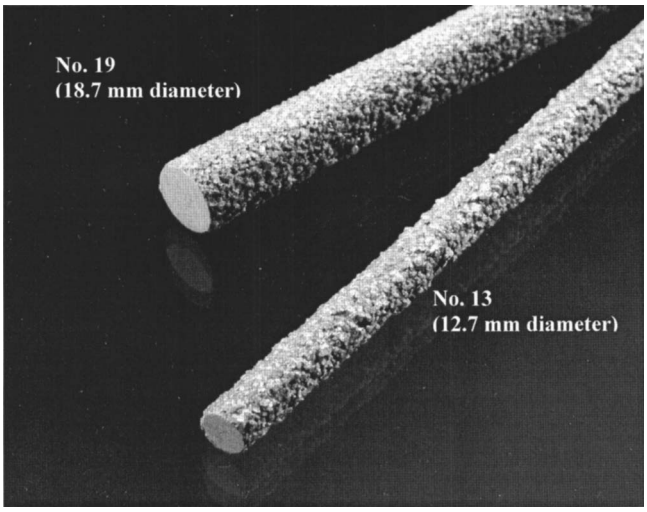

Fig. 1. Glass FRP sand-coated reinforcing bars

Bridge Construction and Details

The Morristown Bridge crosses Ryder Brook on Route 100 in Morristown (Vermont, United States). The bridge has five main steel girders, integrally cast with the two end abutments over a single span of 43.90 m. The deck is a continuous 230 mm thick concrete slab acting compositely with five (60 in. plate girder M270-GR50W) girders spaced at 2.36 m with an overhang of 0.915 m on each side [Fig. 2(a)]. The Morristown Bridge was designed according to serviceability criteria (a maximum crack width of 0.5 mm). The top and bottom mats for the concrete deck slab consisted of GFRP bars. The deck slab was designed according to AASHTO specifications (AASHTO 2000) and ACI design guidelines (*ACI 440.1R-01*), which call for No. 19 GFRP rebar at 100 mm in the top transverse direction and No. 16 GFRP rebar at 100 mm in the bottom transverse direction. This difference between the two layers results from the difference in the concrete cover, which is 64 mm at the top and 38 mm at the bottom [Fig. 2(b)]. The required GFRP reinforcement in the longitudinal direction was No. 16 at 150 mm in the top and the bottom. In keeping with a common practice in bridge engineering and for ease of installation, two identical GFRP mats, No. 19 at 100 and 150 mm in the transverse and longitudinal directions, respectively, were used at the slab top and bottom (Table 2). While the GFRP bars did not require splicing in the transverse direction, an 800 mm splice (about 40 times the bar diameter) in the longitudinal direction was used. The deck was designed without a pavement and stands out as being the first bridge deck in the world of its size and category fully reinforced with GFRP bars. A total of 16,775 m of No. 19 (18.7 mm diameter) GFRP bars went into the bridge deck slab. Construction began in May 2002; the bridge was opened to traffic in September 2002.

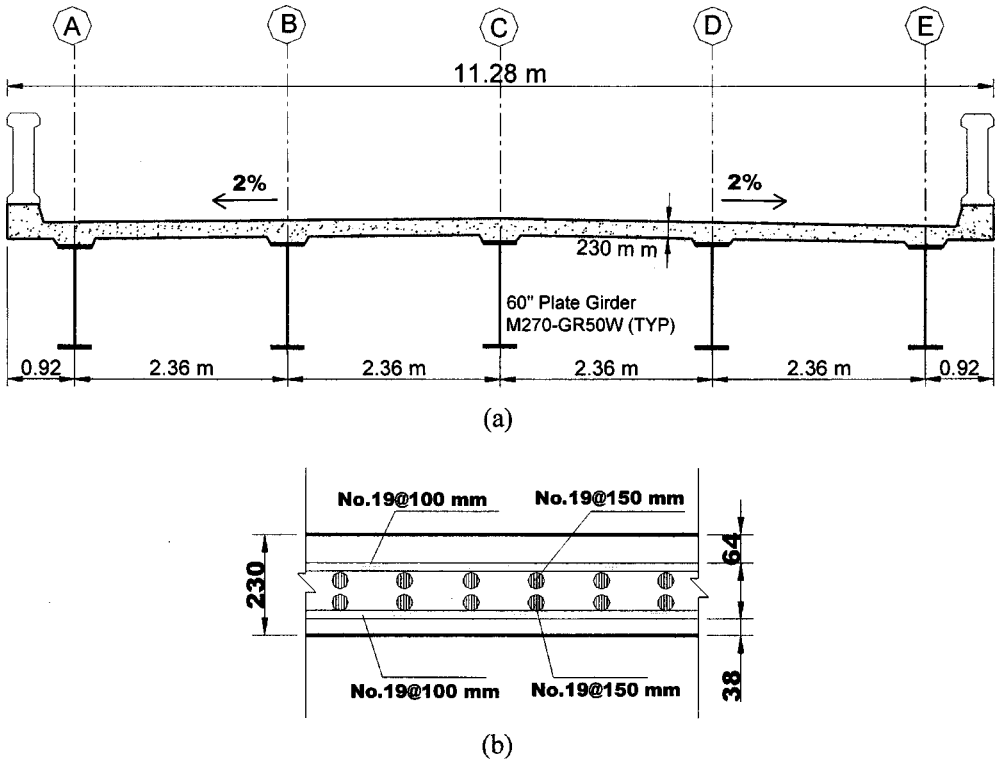

Fig. 2. Cross section and slab reinforcement of Morristown Bridge: (a) Cross section of the bridge; and (b) deck slab reinforcement (transverse section)

FRP Bar Placement

The construction crews reacted positively, indicating that more FRP bars could be handled and placed in less time due to their light weight. Continuous plastic chairs were placed in the longitudinal direction at 0.9 m intervals under the bottom reinforcement mat to support the FRP bars and maintain the required clear concrete cover. In the case of the top mat, single chairs at 0.9 m intervals in both directions were used. The FRP bars withstood all on site handling and placement with no problems. Fig. 3 show photographs of the Morristown Bridge during different stages of construction.

Bridge Instrumentation

The bridge was instrumented at critical locations to measure internal temperature and collect strain data using fiber-optic sensors (FOS). Fabry–Pérot FOSs monitor the strains in the GFRP reinforcement and concrete deck slab, while thermocouples compensate for temperature effects. The FOSs are distributed across the midspan of the bridge. A total of 13 Fabry–Pérot FOSs were used. Eleven FOSs were glued to FRP rebars. Five FOSs were glued to transverse top reinforcement at the bridge midspan at locations of maximum stress over supporting girders [Figs. 4 and 5(a)]. Four FOSs were glued on transverse bottom reinforcement at the bridge midspan at locations of maximum stress midway between girders (Fig. 4). Two FOSs were glued to top longitudinal reinforcement: one on the middle bar on top of the middle girder; the other on the end bar on top of edge girder. Two FOSs were embedded in the concrete at the level of the top and bottom reinforcement. During testing, a system of rulers and theodolites was used to measure concrete slab and girder deflection [Fig. 5(b)].

First Field Load Test

Dynamic and static field tests with calibrated heavy trucks were conducted after construction (mid October 2003) to evaluate stress levels in the FRP reinforcement, concrete deck, and steel girders. The static and dynamic responses of different bridge components have been recorded with computer-aided data logging systems since the bridge opened to traffic.

The Morristown Bridge was tested for service performance under static load using two three-axle calibrated trucks as shown in Fig. 6. The trucks used were approximately equivalent to H-35 and H-32 vehicle load. The bridge was also tested under the dynamic wheel loads of regular traffic. During testing, eight-channel FOS data-acquisition systems (BUS systems) were used

Table 2. GFRP Reinforcement of the concrete deck slab

Main direction (transverse)		Secondary direction (longitudinal)		Overhang (transverse)
Top	Bottom	Top	Bottom	Top
No. 19 at 100 mm (ρ_f=1.95%)	No. 19 at 100 mm (GFRP-1.65%)	No. 19 at 150 mm (ρ_f=1.30%)	No. 19 at 150 mm (ρ_f=1.10%)	No. 19 at 100 mm (ρ_f=1.95%)

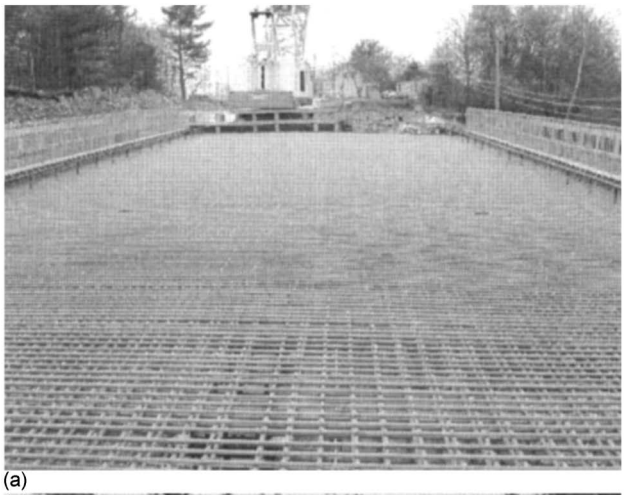

(a)

(b)

(c)

Fig. 3. Construction of Morristown Bridge: (a) FRP reinforcement for the deck slab; (b) bridge deck during casting; and (c) completed bridge

to collect FOS readings. This BUS system was adjusted to collect data at rates of 10 and 500 readings/s during static and dynamic testing, respectively. After testing, a 32-channel FOS data-acquisition system (DMI-32), capable of collecting data at a rate of 10 readings/s, was permanently installed under the bridge for long-term remote monitoring. The slab temperature during testing was 11.5 and 12.5°C at bottom and top, respectively, at the time of static testing.

Four paths (two in each traffic direction, labeled: A, B, C, and D) were marked on the bridge as shown in Fig. 7. Seven stations (stops) at intervals of 7.32 m were also marked along each path to give critical loading cases and influence lines at the instrumented section of the bridge (midspan). The test was carried out using a single truck (Number 1) over the four paths and both trucks simultaneously over two paths (Figs. 7 and 8). A total of 35 readings (7 stations×5 paths) were recorded for each gauge and deflection ruler. Readings were recorded at each truck station when the truck's second axle (first rear axle) was directly over the station.

Test Results

Strains in GFRP Reinforcement

Figs. 9 and 10 show maximum measured tensile strains in the FRP transverse rebars recorded at Gauges B4, T4, B2, and T3 according to truck position along the bridge. The 21.9 value on the horizontal axes represents the location (midspan) of the FOS gauges. The strain values depend on loading, namely, truck position and path. Therefore, for each graph line, the truck path that gives the maximum strain readings is presented. As a result of the truck paths, the single truck was expected to produce maximum strain in the bottom FRP bars and the two trucks together were expected to produce maximum strain in the top FRP bars. For a single truck (Path D), the maximum measured strains in the bottom and top FRP bars were 31 and 4 μstrains, respectively (Fig. 9). In the case of two trucks (Path B-C), the maximum measured strains in the bottom and top FRP bars (readings from the same gauges as in Path D) were 4 and 8 μstrains, respectively (Fig. 10), as predicted. These maximum measured strain values in FRP bars are less than 0.19% of the material's ultimate strain capacity (Table 1). It is worth mentioning here that according to *ACI 440.1R-03* (ACI 2003), the allowable stress (strain) limit for GFRP-reinforced concrete structures exposed to earth and weather, and subjected to fatigue regimes is 14.0% of the material's ultimate stress (strain) capacity.

Dynamic loading produced by regular traffic yielded maximum strain values in FRP reinforcement that were similar to the static tests. Fig. 11 shows the maximum measured strains on the bottom transverse reinforcement caused by a heavy truck crossing the bridge.

Strains in Concrete

The concrete tensile strains can be calculated from the tensile strains measured in the transverse FRP bars. The values of tensile strains at the top (Truck Path B-C at Gauge T3) and bottom (Truck Path D at Gauge B4) surfaces of the concrete slab reached a maximum of 18 and 45 μstrains, respectively. These values were calculated using simple bending theory and considering top and bottom concrete covers of 64 and 38 mm, respectively. The strain values at the concrete surface of the deck slab are well below the cracking strain of concrete, $\varepsilon_{cr}=112$ μstrain (for $f'_c=27$ MPa and $E_c=25$ GPa). After testing, the bridge, which was in service for approximately 13 months before testing, was visually inspected for the development or the opening of cracks.

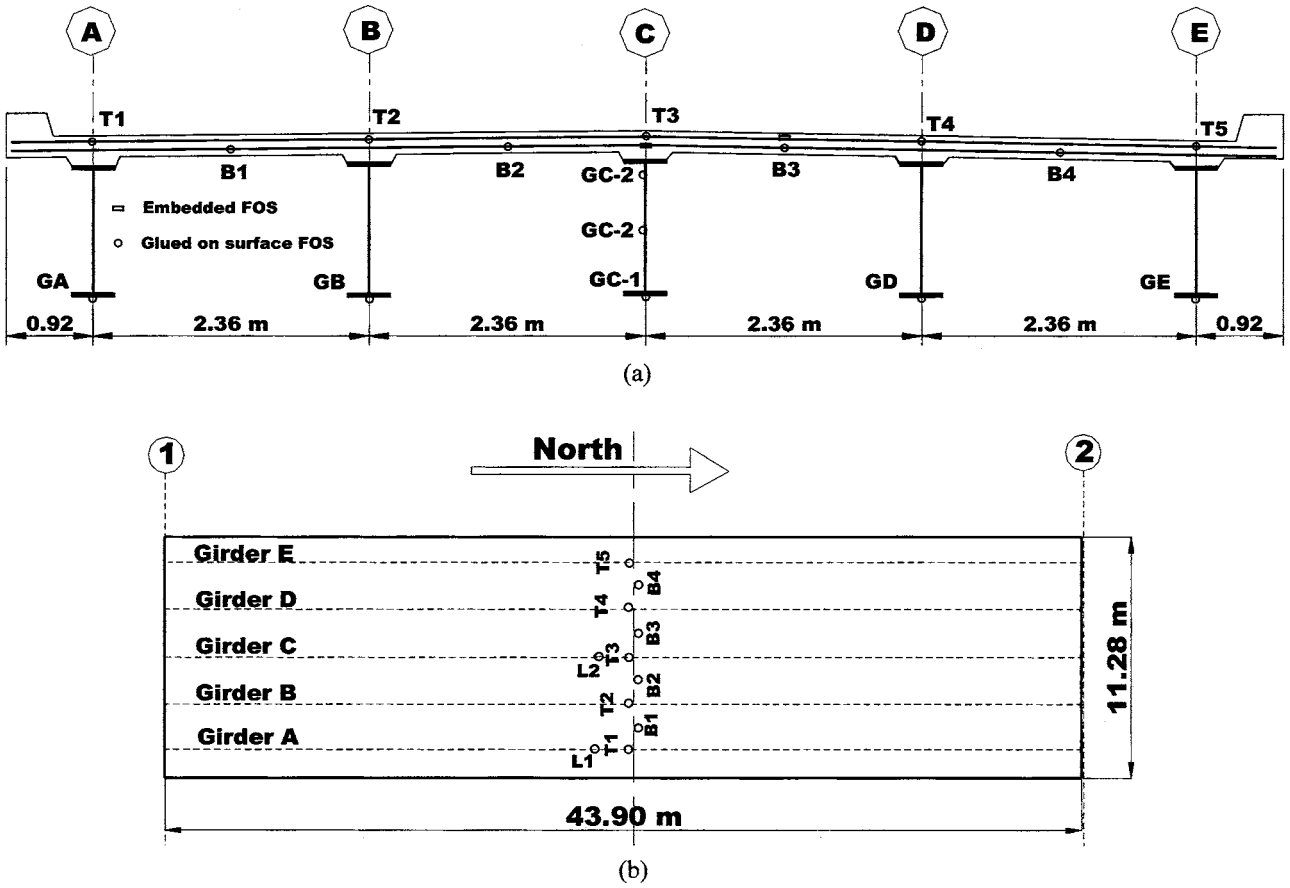

Fig. 4. Schematic drawing for distribution of FOS for strain monitoring: (a) Section elevation; and (b) plan view

No cracks were observed either on the bottom or on the top (the bridge has no insulation or pavement) of the concrete deck slab, which is in agreement with the measured tensile strains in concrete.

It should be noted that the design service wheel load, P_{design}, which equals 114.4 kN (88.0×dynamic factor of 1.3) is greater than the maximum wheel load of the trucks used in the field test, P_{test}, which equals 61.5 kN by approximately 1.86 times. However, if the values of the measured strains from field testing are extrapolated (multiplied by 1.86) the resulting values of tensile strains will be on the order of 58 and 84 μstrain in GFRP bars and concrete, respectively. Therefore, the maximum resulting tensile stresses due to the application of the design wheel load are 2.32 and 2.10 MPa in GFRP bars and concrete, respectively, which are much less than the expected stresses using the flexural design method (64.76 MPa in GFRP bars and more than the tensile strength of concrete—see the Appendix).

These very small strains, both in GFRP bars and in concrete, compared to the expected values according to the flexural design moments suggest that the behavior of the deck slab under concentrated wheel loads is different from what is assumed in design. These results are in good agreement with the previous research work (Hewitt and Batchelor 1975; Fang et al. 1990; Kuang and Morely 1992), which concluded that in bridge decks, the wheel loads are transferred to the supporting girders through arching action and ultimately, which is unlikely to occur in the field, the failure mode would be by punching shear at loads six to seven times the design service wheel loads.

It is now well established that live load strains in the reinforcement of concrete deck slabs keep changing until the slab has developed a stable system of cracks (Bakht and Lam 2000). After the slab has developed a stable system of cracks, it is expected to see higher live load tensile strains in the bottom transverse FRP bars.

Deflection Measurements

During static tests, deflection of the concrete slabs and steel girders was measured with a theodolite and a system of rulers installed at the bridge midspan [Fig. 5(b)]. As shown in Fig. 12, the single truck following Path D (over edge Girder E) produced the peak deflection in Girder E of 7.0 mm (L/6270). The peak deflection with the two calibrated trucks traveling simultaneously along Path B-C was 8.0 mm (L/5490) in Girder B, as shown in Fig. 12.

The deflection of the concrete deck slab was calculated by subtracting the measured value at the slab position from the average of the values measured on the two steel girders adjacent to this position. These maximum recorded values were less than 2 mm (S/1180) and were obtained with one truck traveling the path immediately above the slab position of interest.

Fig. 13 shows the maximum measured deflection of the steel girders at the bridge midspan due to trucks located at midspan in different paths. Note that the truck loading is not evenly distributed on the steel girders. The girder closest to the truck path deforms more than those further away. This was more

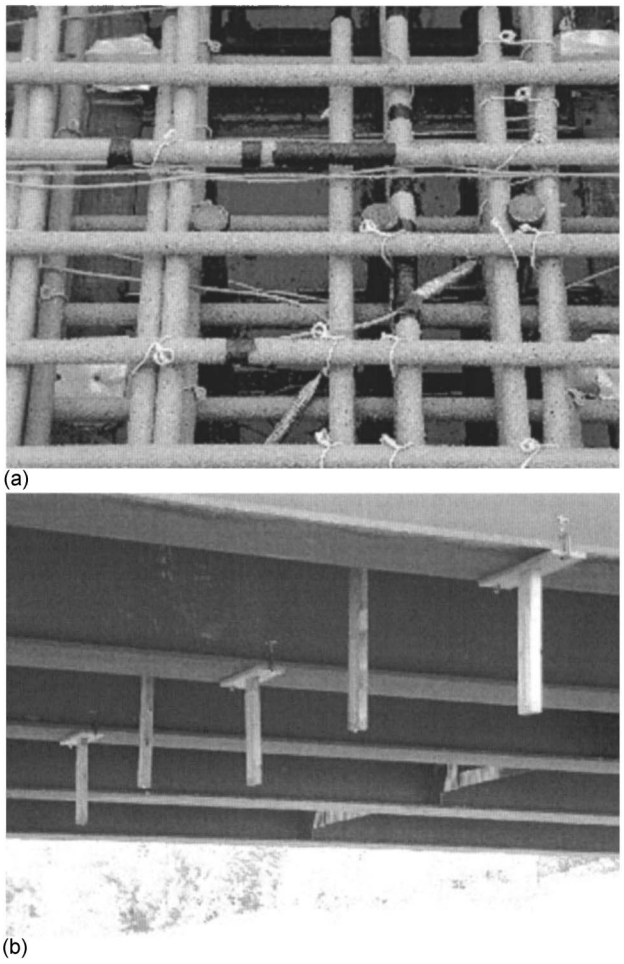

Fig. 5. Instrumentation of Morristown Bridge: (a) Fiber-optic sensors on glass FRP bars; and (b) rulers installed on steel girders to measure deflection

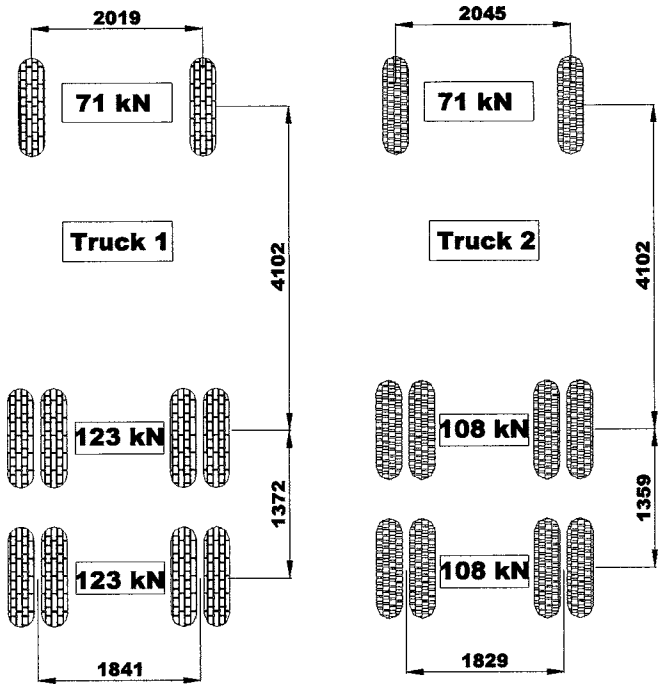

Fig. 6. Truckloads

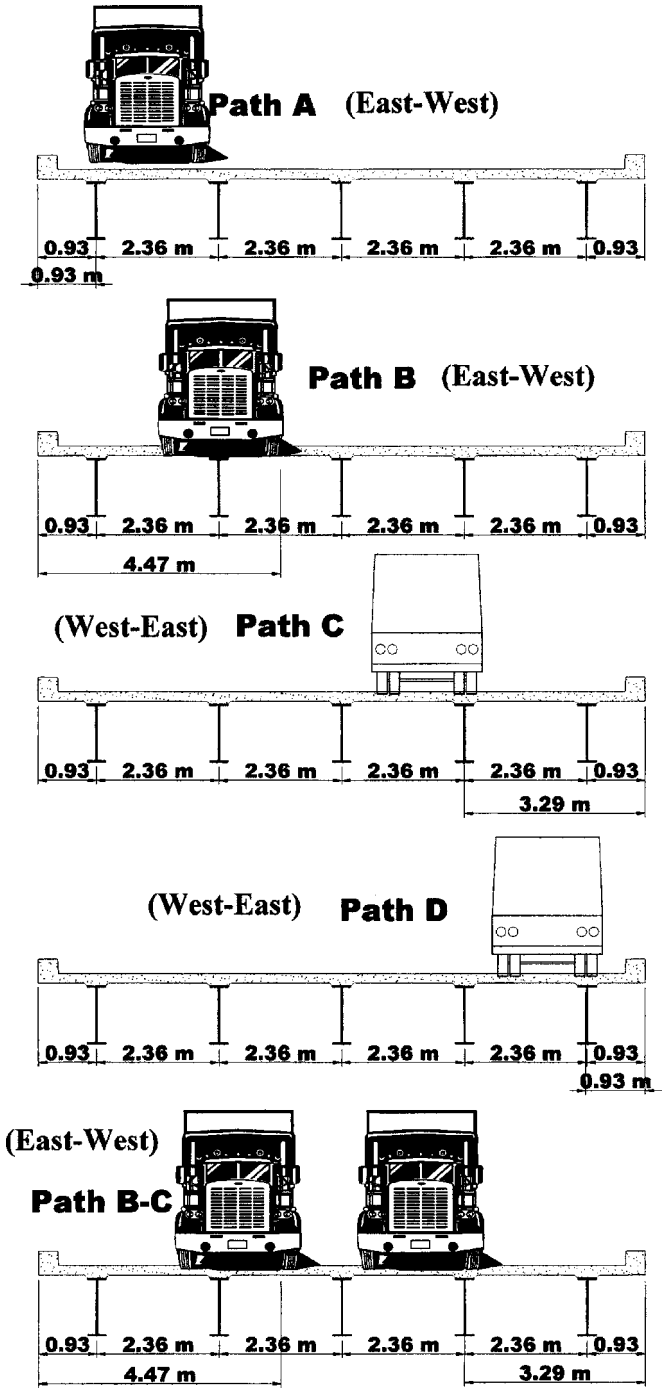

Fig. 7. Paths of trucks during field testing

obvious when the truck traveled over or near the edge girder. For Load Paths B and C, the two intermediate girders directly beneath the truck carry 55–60% of the total load, while the remaining three girders carry 40–45%. These values are 75–80% and 20–25% when the trucks passed over the edge girder (Load Paths A and D).

Live-Load Distribution Factors

Many techniques are available to determine transverse live-load distribution or girder distribution factors (DFs). Zokaie et al. (1991) grouped analytical techniques into three different levels of analysis from detailed modeling to simplified equations. Field

Fig. 8. Field testing of Morristown Bridge

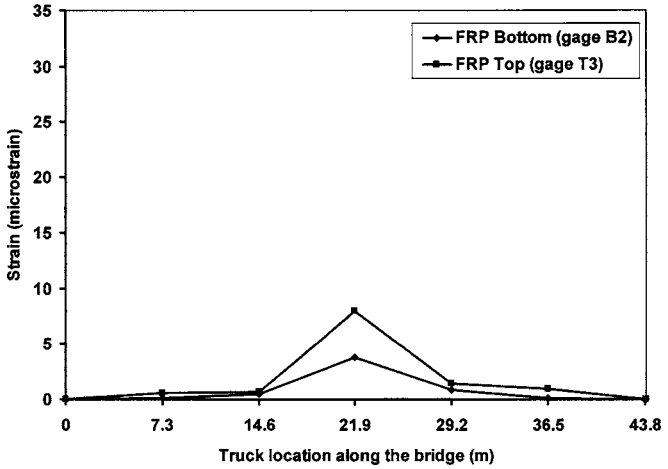

Fig. 10. Maximum tensile strains in FRP bars under wheel loads of two trucks

testing can also provide information on live-load DFs for a given bridge type and geometry (Kim and Nowak 1997; Barr et al. 2001; Eom and Nowak 2001; Schwarz and Laman 2001). The DFs can be determined from field measurements using the following equation:

$$DF_i = \delta_i / \Sigma \delta_i \quad (1)$$

where δ_i=maximum static deflection in the ith girder.

The deflection measurements shown in Fig. 13 are used to determine the live-load distribution factors according to Eq. (1). AASHTO *LRFD Bridge Design Specifications* (AASHTO 1994) provide live-load distribution factors that can be compared to the measured DFs.

The exterior Girder A deflected 7 mm under Truck Path A (Fig. 13). The total deflection of all of the girders was 17 mm for a live-load DF of about 7/17 or 0.41. The AASHTO (1994) live-load distribution factors are 0.61 using the Lever rule and 0.52 with rigid cross-section rotation. These factors are based on load and bridge geometry, and exclude the 1.2 multiple presence factor (AASHTO LRFD Article 4.6.2.2.2d).

The interior Girder B deflected 6 mm under Truck Path B (Fig. 13). The total deflection of all of the girders was 19 mm for a live-load distribution factor of about 6/19 or 0.32. The AASHTO live-load distribution factor is 0.39. The live-load distribution factor depends on girder spacing and span length, and includes the 1.2 multiple presence factor. Removing the multiple presence factor yields a live-load distribution factor of 0.32 (AASHTO LRFD Article 4.6.2.2.2b).

Costs of FRP-Reinforced Bridge Deck

The costs related to using new materials such as GFRP bars stands out as a very important issue. In 2002, the Vermont Agency of Transportation (VTrans) conducted a comparative cost analysis of GFRP and epoxy-coated steel reinforcement for the Morristown Bridge. The results of this analysis revealed

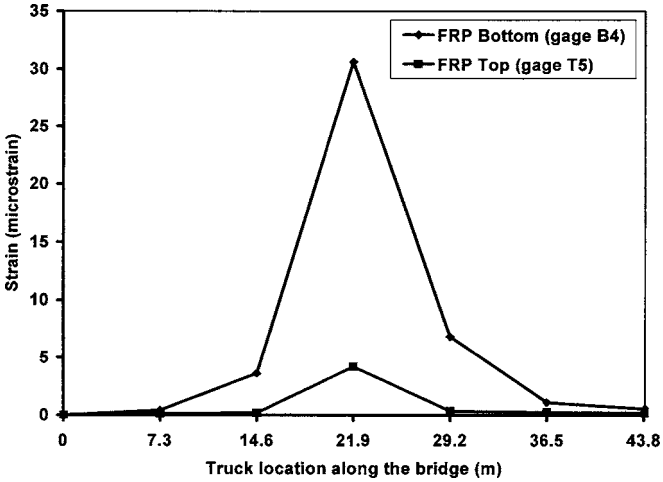

Fig. 9. Maximum tensile strains in FRP bars under wheel loads of one truck (Path D)

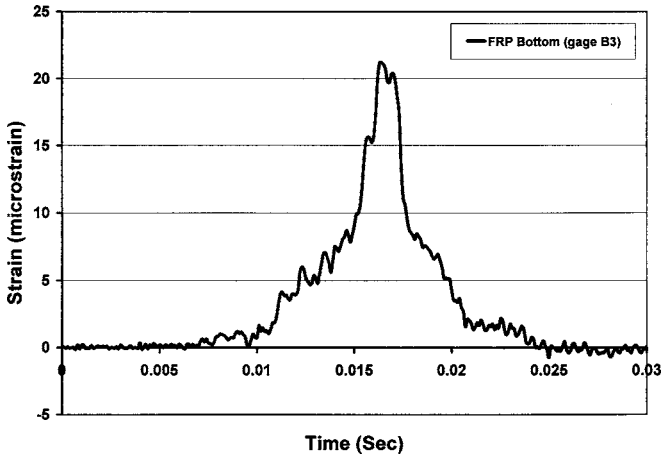

Fig. 11. Maximum tensile strains in bottom FRP bars under dynamic service load

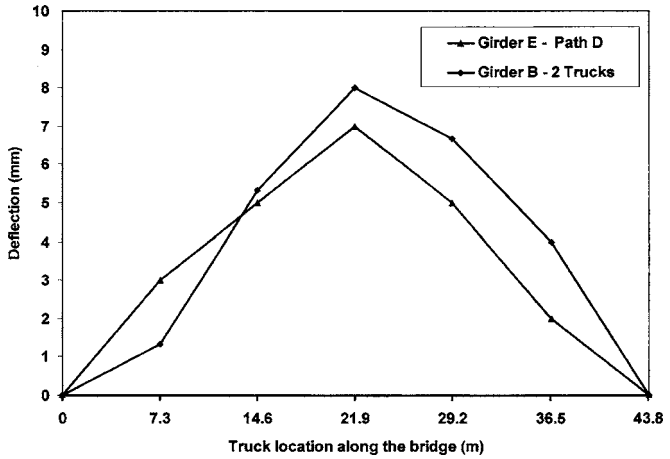

Fig. 12. Deflection of Steel Girders B and E versus truck location

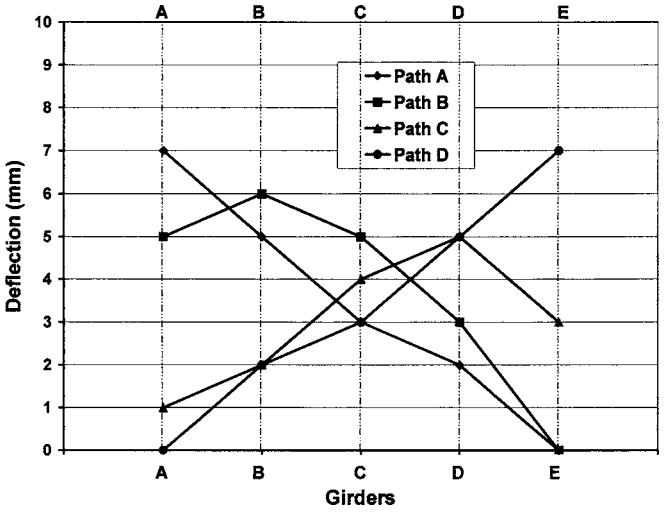

Fig. 13. Maximum measured deflection of steel girders (truck at midspan)

that using GFRP bars will cost $50,000 (United States) more compared to epoxy-coated steel. When reinforcement costs are viewed as a percentage of total bridge cost [$1.40 million (United States)], the actual increase in overall bridge cost with GFRP reinforcement is only 3.57%. Although the increase of the cost was paid through the IBRC (USDOT 2002) program, VTrans engineers expressed satisfaction with the cost increase, stating that the savings in periodic maintenance and repairs over steel reinforced deck slabs more than offset the initial higher cost of GFRP reinforcement.

Conclusions

This paper presented the design, construction details, and test results for the GFRP-reinforced concrete deck of the Morristown Bridge on Route 100 (Vermont, United States). Based on the construction details and the results of the first field loading test, the following conclusions can be drawn:

1. The FRP bars withstood normal on site handling and placement with no problems. In addition, their light weight made them easy to carry and easier to place.
2. As tested, the maximum tensile strains in the GFRP bars were 8 and 31 μstrains, at the top and bottom, respectively. These values represent less than 0.19% of the ultimate strain of the GFRP and suggest that the AASHTO flexural design method overestimates the calculated design moments (service and ultimate).
3. Maximum tensile strain values in the concrete were very small (18–45 μstrains) as the truck moved over the gauge. These values are well below cracking strain for concrete, which is about 112μstrains for 27 MPa normal-weight concrete (E_c=25 GPa).
4. Deck and slab deflections were well below the AASHTO allowable limits. The maximum measured deflection for the steel girders and concrete slabs never exceeded L/5490 (8 mm) and S/1180 (2 mm), respectively, throughout testing.
5. The small measured strains either in GFRP bars or in concrete compared to the expected values according to the flexural design moments suggest that the behavior of the deck slab under concentrated wheel loads is arching action between girders and ultimately, which is unlikely to occur in the field, the failure mode would be by punching shear.
6. The measured girder DFs are in good agreement with live-load distribution factors provided by the AASHTO *LRFD Bridge Design Specifications* (AASHTO 2000).

The construction of Morristown Bridge along with previous field applications (El-Salakawy and Benmokrane 2003; El-Salakawy et al. 2003b) involving bridges of different types and subjected to a variety of environments and service conditions contribute significantly to establishing an optimum design for concrete deck slabs reinforced with noncorrosive FRP bars. Furthermore, the long-term monitoring of strains and temperature using fiber-optic sensors will generate valuable data, which will allow direct comparison with steel reinforcement under actual service conditions. Monitoring and field load tests also provide the ability to collect information about the long-term durability and serviceability performance of FRP concrete bridge decks subjected to real environmental and traffic conditions. In addition, core samples will be extracted periodically from the deck slabs to evaluate the amount of deterioration to the FRP bars and concrete, if any. These field investigations are crucial for proving the durability of innovative structural materials such as GFRP bars.

Acknowledgments

The writers wish to extend special thanks to the following organizations and individuals for their contribution to this project: Pultrall Inc., Division of ADS Composites Group (Thetford Mines, Quebec): supplier of the composite FRP reinforcing bars; Roctest Ltd. (St. Lambert, Quebec): Marco Quirion, supplier of the fiber-optic sensors and data-acquisition system; the Natural Science and Engineering Research Council of Canada (NSERC) (Ottawa, Ontario): partial funding; ISIS-Canada (Network of Centres of Excellence) (Winnipeg, Manitoba): partial funding); Department of Civil Engineering, University of Sherbrooke (Sherbrooke, Quebec); and the Vermont Agency of Transportation: District 6 personnel for field support.

Table 3. Material Properties of Concrete Deck Slab

GFRP bar size	d_b (mm)	A_f (mm^2)	$f_{u,ave}$ (MPa)	f_{fu}^* (guaranteed) (MPa)	E_f (GPa)
16	15.91	198.0	630±27	549.0	42
19	18.72	275.0	597±24	525.0	40

Appendix. Design Calculations of Morristown Bridge Deck Slab

Geometrical Data

- Integral abutment with one span of 43.90 m;
- Two cross-diaphragms spaced at 14.63 m;
- Five steel girders (60 in. Plate Girder M270-GR50W) with a flange width of 0.48 m;
- Span of deck slab 2.36 m;
- Overhang of (used as sidewalk) 0.92 m;
- Slab thickness 230 mm;
- Top clear concrete cover 64 mm; and
- Bottom clear concrete cover 38 mm.

Design Moments Calculated According to AASHTO (2000)

Deck Slab between Girders

- M_u=51.74 kN m/m; and
- M_s=25.93 kN m/m.

Deck Slab at Overhang

- M_u=28.43 kN m/m; and
- M_s=21.80 kN m/m.

For serviceability limit state (calculations of crack width and deflection), the design of the concrete deck slab (Table 3) will be made based on maximum crack width of 0.5 mm. To calculate crack width or deflection the equations given in *ACI-440.1R-03* design guidelines, when applicable, will be used.

Balanced reinforcement ratio (*ACI-440.1R-03*)

$$\rho_{fb} = 0.85\beta_1 \frac{f'_c}{f_{fu}} \frac{E_f \varepsilon_{cu}}{E_f \varepsilon_{cu} + f_{fu}}$$

$$\beta_1 = 0.85 \quad (f_c = 27 \text{ MPa})$$

$$\rho_{fb} = 0.85 \frac{27}{525}(0.85) \frac{(40{,}000)(0.003)}{(40{,}000)(0.003) + 525} = 0.691\%$$

Deck Slab between Girders (Fig. 14)

- Top surface (M_s=25.93 kN m, clear concrete cover=64 mm);
- Serviceability limit state; and
- Try GFRP bars No. 19 at 100 mm
  Effective depth: d=230–64–18.8/2=156.6 mm
  ρ_f=275/(100×156.6)=1.76%>ρ_{fb}=0.691%
  (the section is over-reinforced).

Cracking

$$n_f = \frac{E_f}{E_c} = \frac{40{,}000}{25{,}000} = 1.6$$

$$k = \sqrt{2\rho_f n_f + (\rho_f n_f)^2} - \rho_f n_f = 0.211$$

$$f_f = \frac{M_s}{A_f d\left(1 - \frac{k}{3}\right)} = \frac{25.93}{10 \times 0.000275(0.1566)\left(1 - \frac{0.211}{3}\right)}$$

$$= 64.76 \text{ MPa}$$

$$d_c = (h - d) = 230 - 156.6 = 73.4 \text{ mm}$$

For design purposes, the maximum clear concrete cover is 50 mm

$$d_c = 50 + 18.8/2 = 59.4 \text{ mm}$$

$$A = \frac{2 d_c b}{\text{number of bars}} = \frac{2(59.4)(1{,}000)}{10} = 11{,}880 \text{ mm}^2$$

$$\beta = \frac{h - kd}{d - kd} = \frac{0.230 - 0.211(0.1566)}{0.1566 - 0.211(0.1566)} = 1.59 \quad \text{and} \quad k_b = 1.0$$

$$w = \frac{2.2}{E_f} \beta k_b f_f \sqrt[3]{d_c A} = \frac{2.2}{40 \times 10^3}(1.59)(1.0)(64.76)\sqrt[3]{(59.4)(11{,}880)}$$

$$w = 0.504 \text{ mm} \sim 0.50 \text{ mm} \quad \text{OK}$$

Ultimate Limit State

M_u=51.74 kN m (top and bottom moment)

$$f_f = \left[\sqrt{\frac{(E_f \varepsilon_{cu})^2}{4} + \frac{0.85\beta_1 f'_c}{\rho_f} E_f \varepsilon_{cu}} - 0.5 E_f \varepsilon_{cu} \right]$$

×(for over-reinforced section)

$$f_f = \sqrt{\frac{(40 \times 10^3 \times 0.003)^2}{4} + \frac{0.85 \times 0.85 \times 27}{0.0176}(40 \times 10^3)(0.003)} - 0.5(40 \times 10^3)(0.003) = 309.6 \text{ MPa}$$

$$M_n = \rho_f f_f \left(1 - 0.59 \frac{\rho_f f_f}{f'_c}\right) b d^2 = 117.71 \text{ kN m}$$

Strength reduction factor, ϕ=0.7 (over-reinforced section)

$$\phi M_n = 82.40 \text{ kN m} > 51.74 \text{ kN m} \quad \text{OK}$$

Check for Creep Rupture

Unfactored sustained moment,

$M_{sus}=M_d+0.2M_l=4.61+0.2\times21.32=8.87$ kN m

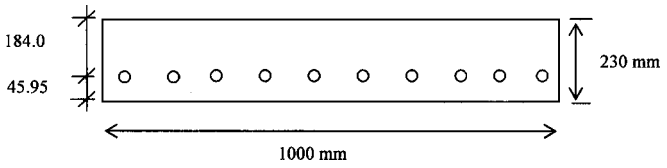

Fig. 14. Deck slab between girders

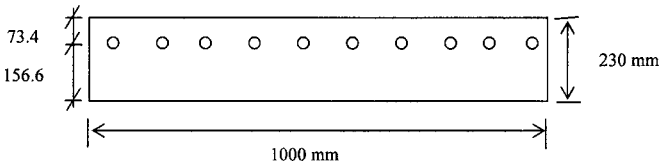

Fig. 15. Deck slab over girders

$$f_f = \frac{M_{sus}}{A_f d\left(1 - \frac{k}{3}\right)} = \frac{8.87}{10 \times 0.000275(0.1566)\left(1 - \frac{0.211}{3}\right)}$$

$$= 22.16 \text{ MPa}$$

$$22.16 \text{ MPa} \leqslant 0.2 \times 0.70 \times 525 = 73.5 \text{ MPa} \quad \text{OK}$$

- Bottom surface (M_s=25.93 kN m, clear concrete cover =38 mm);
- Serviceability limit state;
- Try GFRP bars No. 16 at 100 mm (Fig. 15);
- Effective depth: d=230−38−15.9/2=184.05 mm; and
- ρ_f=198/(100×184.05)=1.076%>ρ_{fb}=0.886% (the section is over-reinforced).

Cracking

$$n_f = \frac{E_f}{E_c} = \frac{42{,}000}{25{,}000} = 1.68$$

$$k = \sqrt{2\rho_f n_f + (\rho_f n_f)^2} - \rho_f n_f = 0.172$$

$$f_f = \frac{M_{ser}}{A_f d\left(1 - \frac{k}{3}\right)} = \frac{25.93}{198 \times 10^{-6} \times (0.18405)\left(1 - \frac{0.172}{3}\right)}$$

$$= 75.48 \text{ MPa}$$

$$d_c = (h - d) = 230 - 184.05 = 45.95 \text{ mm}$$

$$A = \frac{2d_c b}{\text{number of bars}} = \frac{2(45.95)(1{,}000)}{10} = 9{,}190 \text{ mm}^2$$

$$\beta = \frac{h - kd}{d - kd} = \frac{0.23000 - 0.197(0.18405)}{0.18405 - 0.197(0.18405)} = 1.3 \quad \text{and} \quad k_b = 1.0$$

$$w = \frac{2.2}{E_f}\beta k_b f_f \sqrt[3]{d_c A} = \frac{2.2}{42 \times 10^3}(1.3)(1.0)(75.48)\sqrt[3]{(45.95)(9{,}190)}$$

$$w = 0.385 \text{ mm} < 0.50 \text{ mm} \quad \text{OK}$$

Ultimate Limit State

M_u=51.74 kN m (top and bottom moment)

$$f_f = \left[\sqrt{\frac{(E_f \varepsilon_{cu})^2}{4} + \frac{0.85\beta_1 f'_c}{\rho_f} E_f \varepsilon_{cu}} - 0.5 E_f \varepsilon_{cu}\right]$$

×(for over-reinforced section)

$$f_f = \sqrt{\frac{(42 \times 10^3 \times 0.003)^2}{4} + \frac{0.85 \times 0.85 \times 27}{0.0107}(42 \times 10^3)(0.003)} - 0.5(42 \times 10^3)(0.003) = 420.40 \text{ MPa}$$

$$M_n = \rho_f f_f\left(1 - 0.59\frac{\rho_f f_f}{f'_c}\right)bd^2 = 137.39 \text{ kN m}$$

Strength reduction factor, ϕ=0.7 (over-reinforced section)

$$\phi M_n = 96.17 \text{ kN m} > 51.74 \text{ kN m} \quad \text{OK}$$

Check for Creep Rupture

Unfactored sustained moment,
$M_{sus}=M_d+0.2M_l=4.61+0.2\times21.32=8.87$ kN m

$$f_f = \frac{M_{sus}}{A_f d\left(1 - \frac{k}{3}\right)} = \frac{8.87}{10 \times 0.000198(0.18405)\left(1 - \frac{0.172}{3}\right)}$$

$$= 25.82 \text{ MPa}$$

$$25.82 \text{ MPa} \leqslant 0.2 \times 0.70 \times 549 = 76.86 \text{ MPa} \quad \text{OK}$$

Deck Slab at Overhang

- Serviceability limit state

$$M_s = 21.80 \text{ kN m (top moment)}$$

- Use the same top GFRP bars No. 19 at 100 mm
  Effective depth: d=230−38−18.8/2=182.6 mm
  ρ_f=275/(100×182.6)=1.50%>ρ_{fb}=0.886% (the section is over-reinforced)

Cracking

$$k = \sqrt{2\rho_f n_f + (\rho_f n_f)^2} - \rho_f n_f = 0.197$$

$$f_f = \frac{M_s}{A_f d\left(1 - \frac{k}{3}\right)} = \frac{21.80}{2{,}750 \times 10^{-6} \times (0.1826)\left(1 - \frac{0.197}{3}\right)}$$

$$= 46.46 \text{ MPa}$$

$$d_c = (h - d) = 230 - 182.6 = 47.4 \text{ mm}$$

$$A = \frac{2d_c b}{\text{Number of bars}} = \frac{2(47.4)(1{,}000)}{10} = 9{,}480 \text{ mm}^2$$

$$\beta = \frac{h - kd}{d - kd} = \frac{0.2300 - 0.197(0.1826)}{0.1826 - 0.197(0.1826)} = 1.32 \text{ and } k_b = 1.0$$

$$w = \frac{2.2}{E_f}\beta k_b f_f \sqrt[3]{d_c A} = \frac{2.2}{40 \times 10^3}(1.32)(1.0)(46.46)\sqrt[3]{(47.4)(9{,}480)}$$

$$w = 0.259 \text{ mm} < 0.50 \text{ mm} \quad \text{OK}$$

Ultimate Limit State

$M_u = 28.43$ kN m (top moment)

$$f_f = \left[\sqrt{\frac{(E_f \varepsilon_{cu})^2}{4} + \frac{0.85\beta_1 f'_c}{\rho_f}E_f \varepsilon_{cu}} - 0.5E_f \varepsilon_{cu}\right]$$

$\times$(for over-reinforced section)

$$f_f = \sqrt{\frac{(40 \times 10^3 \times 0.003)^2}{4} + \frac{0.85 \times 0.85 \times 27}{0.015}(40 \times 10^3)(0.003)} - 0.5(40 \times 10^3)(0.003) = 339.57 \text{ MPa}$$

$$M_n = \rho_f f_f\left(1 - 0.59\frac{\rho_f f_f}{f_c}\right)bd^2 = 150.93 \text{ kN m}$$

Strength reduction factor, $\phi = 0.7$ (over-reinforced section)

$$\phi M_n = 105.65 \text{ kN m} > 28.43 \text{ kN m} \quad \text{OK}$$

Check for Creep Rupture

Unfactored sustained moment,
$M_{sus} = M_d + 0.2M_l = 4.39 + 0.2 \times 17.40 = 7.87$ kN m

$$f_f = \frac{M_{sus}}{A_f d\left(1 - \frac{k}{3}\right)} = \frac{7.87}{10 \times 0.000275(0.1826)\left(1 - \frac{0.197}{3}\right)}$$

$$= 16.78 \text{ MPa}$$

$$16.78 \text{ MPa} \leq 0.2 \times 0.70 \times 525 = 73.5 \text{ MPa} \quad \text{OK}$$

Notation

The following symbols are used in this paper:

- A = effective tension area of concrete surrounding main tension reinforcement with its centroid coincides with reinforcement, divided by number of bars (mm^2);
- A_f = nominal cross-sectional area of FRP bars (mm^2);
- b = width of slab strip considered for design (mm);
- d = effective depth of tensile reinforcement (mm);
- d_b = nominal diameter of bar (mm);
- d_c = thickness of concrete cover measured from extreme tension fiber to center of longitudinal bar located closest thereto (mm);
- E_c = modulus of elasticity of concrete (GPa);
- E_f = modulus of elasticity of FRP bar (GPa);
- f'_c = compressive strength of concrete (MPa);
- f_f = stress in FRP reinforcement at specified loads, calculated by elastic cracked section theory (MPa);
- f_{fu} = design tensile strength of FRP reinforcing bars considering reduction for service environment (MPa);
- f^*_{fu} = guaranteed tensile strength of FRP reinforcing bars, defined as mean tensile strength of sample of test specimens minus three times standard deviation (MPa);
- $f_{u,\text{ave}}$ = mean tensile strength of f a sample of test specimens (MPa);
- h = overall height of slab cross section (mm);
- h_1 = distance from centroid of tension reinforcement to neutral axis (mm);
- h_2 = distance from extreme tension fiber to neutral axis (mm);
- k = ratio of depth of neutral axis to reinforcement depth;
- k_b = bond-dependent coefficient;
- M_d = moment due to dead loads (kN m);
- M_l = moment due to live loads (kN m);
- M_n = nominal moment capacity (kN m);
- M_s = moment at service condition (kN m);
- M_u = factored moment at section (kN m);
- m = number of bars;
- n_f = ratio of modulus of elasticity of FRP bars to modulus of elasticity of concrete;
- w = crack width (mm);
- β = ratio of distance from neutral axis to extreme tension fiber to distance from neutral axis to center of tensile reinforcement;
- β_1 = factor taken as 0.85 for concrete strength f'_c up to and including 28 MPa. For strength above 28 MPa, this factor is reduced continuously at rate of 0.05 per each 7 MPa of strength in excess of 28 MPa, but is not taken less than 0.65;
- ε_{cu} = maximum usable compressive strain in concrete;
- ρ_f = actual FRP reinforcement ratio;
- ρ_{fb} = FRP reinforcement ratio producing balanced strain conditions; and
- ϕ = strength reduction factor.

References

American Association of State Highway and Transportation Officials (AASHTO). (1994). *LRFD bridge design specifications*, 1st Ed., AASHTO, Washington, D.C.

American Association of State Highway and Transportation Officials (AASHTO). (2000). *Standard specifications for design of highway bridges*, AASHTO, Washington, D.C.

American Concrete Institute (ACI). (2003). *Guide for the design and construction of concrete reinforced with FRP bars, ACI-440.1R-03*, ACI, Farmington Hills, Mich.

Bakht, B., and Lam, C. (2000). "Behavior of transverse confining systems for steel-free deck slabs." *J. Bridge Eng.*, 5(2), 139–147.

Barr, P. J., Eberhard, M. O., and Stanton, J. F. (2001). "Live-load distribution factors in prestressed concrete girder bridges." *J. Bridge Eng.*, 6(5), 298–306.

Benmokrane, B., and El-Salakawy, E., eds. (2002). "Durability of fiber reinforced polymer (FRP) composites for construction." *Proc., 2nd Int. Conf.*, Montréal.

Benmokrane, B., and Rahman, H., eds. (1998). "Durability of fiber reinforced polymer (FRP) composites for construction." *Proc., 1st Int. Conf.*, Sherbrooke, Que., Canada.

Benmokrane, B., Rahman, H., Mukhopadhyaya, R., Masmoudi, R., Zhang, B., Lord, I., and Tadros, G. (2001a). "Fiber-optic sensors monitor FRP-reinforced bridge." *ACI Int.*, 23(6), 33–38.

Benmokrane, B., Ton-That, M. T., Laoubi, K., Robert, J. F., and Wang, P. (2001b). "Durability evaluation of glass FRP composites rods in concrete environment." *Proc., 3rd Int. Conf. on Concrete Under Severe Conditions: Environment and Loading*, Vancouver, Canada, Vol. 2, 1239–1246.

Benmokrane, B., Wang, P., Ton-That, T. M., Rahman, H., and Robert, J.-F. (2002a). "Durability of GFRP reinforcing bars in concrete environment." *J. Compos. Constr.*, 6(3), 143–153.

Benmokrane, B., Zhang, B., Laoubi, K., Tighiouart, B., and Lord, I. (2002b). "Mechanical and bond properties of new generation of carbon fiber reinforced polymer reinforcing bars for concrete structures." *Can. J. Civ. Eng.*, 29(2), 338–343.

Bradberry, T. E. (2001). "Concrete bridge decks reinforced with fiber reinforced polymer bars." *Transportation Research Record 1770*, Transportation Research Board, Washington, D.C., 94–104.

Bradberry, T. E., and Wallace, S. (2003). "FRP reinforced concrete in Texas transportation—Past, present, future." *American Concrete Institute Special Publication, Field Applications of FRP Reinforcement: Case Studies*, *SP-215-1*, American Concrete Institute, Farmington Hills, Mich., 3–36.

Canadian Standards Association International (CSA Int.). (2000). "Canadian highway bridge design code."*CAN/CSA-S6-00*, CSA Int., Rexdale, Toronto.

Canadian Standards Association International (CSA Int.). (2002). "Design and construction of building components with fiber reinforced polymers."*CSA S806-02*, CSA Int., Rexdale, Toronto.

El-Salakawy, E., and Benmokrane, B. (2003). "Design and testing of a highway concrete bridge deck reinforced with glass and carbon FRP bars." *American Concrete Institute Special Publication, Field Applications of FRP Reinforcement: Case Studies*, *SP-215-2*, American Concrete Institute, Farmington Hills, Mich., 37–54.

El-Salakawy, E. F., and Benmokrane, B. (2004). "Serviceability of concrete bridge deck slabs reinforced with FRP composite bars." *ACI Struct. J.*, 101(5), 593–602.

El-Salakawy, E. F., Benmokrane, B., Brière, F., Masmoudi, R., and Beaumier, E. (2003a). "Concrete bridge barriers reinforced with GFRP composite bars." *ACI Struct. J.*, 100(6), 815–824.

El-Salakawy, E., Benmokrane, B., and Desgagné, G. (2003b). "FRP composite bars for the concrete deck slab of Wotton Bridge." *Can. J. Civ. Eng.*, 30(5), 861–870.

Eom, J., and Novak, A. S. (2001). "Live load distribution for steel girder bridges." *J. Bridge Eng.*, 6(6), 489–497.

Fang, I. K., Worley, J., Burns, N. H., and Klingner, R. E. (1990). "Behavior of isotropic R/C bridge decks on steel girders." *J. Compos. Constr.*, 116(3), 659–678.

GangaRao, H. V. S., Thippesway, H. K., Kumar, S. V., and Franco, J. M. (1997). "Design, construction and monitoring of the first FRP reinforced concrete bridge deck in the United States." *Proc., 3rd Int. Symp. (FRPRCS 3) on Non-Metallic (FRP) Reinforcement for Concrete Structures*, Sapporo, Japan, Vol. 1, 647–656.

Hassan, T., Rizkalla, S., Abdelrahman, A., and Tadros, G. (1999). "Design recommendations for bridge deck slabs reinforced by fiber reinforced polymers." *Proc., 4th Int. Symp. on Fiber Reinforced Polymers Reinforcement for Concrete Structures, FRPRCS-4, ACI-SP-188*, Baltimore, Md., 313–323.

Hewitt, B. E., and Batchelor, B. (1975). "Punching shear strength of restrained slabs." *J. Struct. Div. ASCE*, 101(9), 1837–1853.

Huckelbridge, A. A., and Eitel, A. K. (2003). "Preliminary performance observations for FRP reinforced concrete bridge deck." *American Concrete Institute Special Publication, Field Applications of FRP Reinforcement: Case Studies*, *SP-215-7*, American Concrete Institute, Farmington Hills, Mich., 121–138.

Humar, J., and Razaqpur, G., eds. (2000). "Advanced composite materials in bridges and structures." *Proc., 3rd Int. Conf.*, Ottawa.

Intelligent Sensing for Innovative Structures Canada (ISIS Canada). (2001). "Reinforcing concrete structures with fiber reinforced polymers."*ISIS-M03-01*, The Canadian Network of Centers of Excellence on Intelligent Sensing for Innovative Structures, Univ. of Winnipeg, Manitoba, Canada.

Japan Concrete Institute. (1997). "Non-metallic (FRP) reinforcement for concrete structures." *Proc., 3rd Int. Symp. (FRPRCS-3)*, Sapporo, Japan, Vol. 1.

Khanna, S., Mufti, A., and Bakht, B. (2000). "Experimental investigation of the role of reinforcement in the strength of concrete deck slabs." *Can. J. Civ. Eng.*, 27(5), 475–480.

Kim, S., and Nowak, A. S. (1997). "Load distribution and impact factors for I-girder bridges." *J. Bridge Eng.*, 2(3), 97–104.

Kuang, J. S., and Morely, C. T. (1992). "Punching shear behavior of restrained reinforced concrete slabs." *ACI Struct. J.*, 89(1), 13–19.

Laoubi, K., El-Salakawy, E. F., Pigeon, M., and Benmokrane, B. (2003). "Durability of concrete beams reinforced with GFRP bars under different environmental and loading conditions." *Proc., 6th Int. Symp. on Fibre Reinforced Polymer (FRP) Reinforcement for Concrete Structures (FRPRCS-6)*, Singapore.

Nanni, A., and Faza, S. (2002). "Designing and constructing with FRP bars: An emerging technology." *ACI Concrete Int.*, 24(11), 53–58.

Nkurunziza, G., Cousin, P., Masmoudi, R., and Benmokrane, B. (2003). "Effect of sustained tensile stress and alkaline on durability of GFRP bars." *Int. J. Mater. Prod. Technol.*, 19(4&5), 1–13.

Rizkalla, S., Shehata, E., and Abdelrahman, A. (1998). "Design and construction of a highway bridge reinforced for shear and prestressed by CFRP." *Proc., American Concrete Institute Seminar on Field Applications of FRP Reinforcement to Concrete: Part I and Part II*, Atlanta.

Rizkalla, S., and Tadros, G. (1994). "First smart bridge in Canada." *ACI Concrete Int.*, 16(6), 42–44.

Saadatmanesh, H., and Ehsani, M. R., eds. (1996). "International conference on composites for infrastructure." *Proc., ICCI*, Tucson, Ariz., 340.

Schwarz, M., and Laman, J. A. (2001). "Response of prestressed concrete I-girder bridges to live load." *J. Bridge Eng.*, 6(1), 1–8.

Steffen, R. E., Trunfio, J. P., and Bowman, M. M. (2001). "Performance of a bridge deck reinforced with CFRP grids in Rollinsford, New Hampshire, USA." *Proc., CCC 2001, FRP Composites in Construction*, J. Figueiras, L. Juvandes, and R. Furia, eds., Porto, Portugal, 671–676.

Stone, D., Nanni, A., and Myers, J. J. (2001). "Field and laboratory performance of FRP bridge decks." *Proc., CCC 2001, FRP Composites in Construction*, J. Figueiras, L. Juvandes, and R. Furia, eds., Porto, Portugal, 701–706.

Tadros, G. (2000). "Provisions for using FRP in the Canadian highway bridge design code." *ACI Concrete Int.*, 22(7), 42–47.
United States Department of Transportation (USDOT). (2002). "FRP composite bridge technology." USDOT Federal Highway Administration, ⟨www.fhwa.dot.gov/bridge/frp/frpintro.html⟩ (August 19, 2002).
Wang, P., Masmoudi, R., and Benmokrane, B. (2002). "Durability of GFRP composite bars for concrete structures: Assessment and improvement." *Proc., 2nd Int. Conf. on Durability of FRP Composites for Construction, CDCC'2002*, Montreal, 153–164.
Yost, J. R., and Schmeckpeper, E. R. (2001). "Strength and serviceability of FRP grid reinforced bridge decks." *J. Bridge Eng.*, 6(6), 605–612.
Yunovich, M., and Thompson, N. (2003). "Corrosion of highway bridges: Economic impact and control methodologies." *ACI Concrete Int.*, 25(1), 52–57.
Zokaie, T., Osterkamp, T. A., and Imbsen, R. A. (1991). "Distribution of wheel loads on highway bridges." *Final Rep. NCHRP 12-26/1*, National Cooperative Highway Research Program, Washington, D.C.